Analysis of Bridge Structures Crossing Fault Rupture Zones: Seismic Ground Motion Simulation

Douglas Dreger, Gabriel Hurtado, and Anil K. Chopra
University of California Berkeley

Abstract

Bridges that cross faults are subject to static deformation that occurs close in time to the arrival of dynamic pulse-like ground motions. Static offsets can be as large as several centimeters to 10s of meters and strong ground motion velocity pulses exceeding 100 cm/s have been observed. Near-fault records, in the distance range of 10 to 100s of meters from faults are essentially nonexistent except for a few cases, and therefore numerical simulation of ground motions for such near-fault situations is necessary. We simulate ground motions to 17.5 Hz, 15-100m from the fault for a Mw6.5 earthquake using a finite-difference code. Simulations for homogeneous Earth structure are compared for uniform and heterogeneous fault rupture scenarios. Synthetic records for these idealized scenarios are used as input for the analysis of bridges crossing fault rupture zones, and that work is presented in the companion paper entitled "Estimation of Seismic Demands in Bridges Crossing Fault Rupture Zones."

Introduction

Bridges that cross faults can be subjected to large dynamic and static ground motions. As there are very few actual ground motions recorded very close to ruptured faults (< 100m) ground motion simulation is the only viable way to obtain time histories for structural analysis. In this paper, and the companion study entitled 'Estimation of Seismic Demands in Bridges Crossing Fault Rupture Zones,' by Professors Goel and Chopra the objective is to analyze the response of bridges due to representative near-fault ground motion time histories, and as is described in the companion paper use this information to develop a simplified procedure for incorporating fault offset in the design of bridges. In this paper the simulation of the input ground motion time histories is presented.

In our application, bridges with a minimum span of 30m are considered. Ground motion simulations were carried out with this separation in mind and the motions were computed with a closest distance to the fault of 15m. The simulated time histories must accurately incorporate the near-fault source radiation pattern, account for far- and near-field seismic radiation, and have the ability to characterize motions for a broad range of fault types (e.g. vertical strike-slip and reverse faulting), as well as variable slip and full kinematic description of the rupture process. We must be able to accurately simulate the directivity effect as well as the sudden elastic rebound sometimes referred to as fling. The 3D elastic finite-difference code e3d (Larsen and Schultz, 1995) satisfies these requirements and has

undergone validation testing as part of the PEER/SCEC project to validate numerical algorithms for ground motion simulation. Because of the need to compute motions very close to the fault and at high frequency this poses a significant computational challenge.

Simulation Method

The simulation method that we use is a 4th order accurate staggered-grid finite-difference code, e3d, developed at Lawrence Livermore National Laboratory (LLNL) (Larsen and Schultz, 1995). Stress-free boundary conditions are used to model the free surface, and absorbing boundary conditions are used to damp artificial reflections from the grid boundary. This code was tested and calibrated in a PEER/SCEC funded effort to validate numerical methods for ground motion simulation. We have used this code in numerous studies of three-dimensional ground motion modeling (Stidham et al., 1999; Panning et al., 2000; Dolenc et al., 2005) as well as in ongoing work studying the Santa Clara Valley and the Napa Valley.

The advantage of using a finite-difference code is that it is capable of simulating complete seismic waveforms in three-directions of motion that are complete in terms of near-, intermediate, and far-field terms of the solution to the elasto-dynamic equation of motion. We use a high spatial resolution (fine grid discretization) to obtain the motions close to the fault. The high spatial resolution also improves the representation of the kinematic rupture process by allowing smooth evolution of the propagating rupture front and slip rise time on the fault. The obvious benefit of this approach is that the source representation resolution is the same as in the ground motion computation. Finally, the method also allows the straightforward incorporation of rupture heterogeneity and seismic velocity structure including 3D velocity structure if warranted.

In this project we have started out with simplified models consisting of an elastic half-space and uniform slip distribution in order to develop a set of characteristic near-fault time histories. In this case, the numerical method we employ is ‘over-kill’, however as previously stated, it is possible to use more complicated models later if required. Perhaps most importantly the simulated time histories for all levels of approximation will be computed with the same numerical code providing consistency.

The source model described in more detail below consists of a uniform slip rupture at 80% of the shear wave velocity as is commonly observed in finite-source inversion studies of moderate earthquakes. We have also produced simulations with other values of the rupture velocity including super shear rupture velocity, and we are in the process of setting up simulations using a kinematic representation of a variable slip source model. An overview of the preliminary simulation results are provided in this paper and additional details will be presented at the Caltrans Bridge Research Conference.

Model Parameters

We simulated ground motions for a Mw6.5 event assuming a hard rock, elastic half-space velocity model with Vp, Vs and density equal to 6.0 km/s, 3.5 km/s and 2.67 g/cc,

respectively. Because of the close proximity to the ruptured fault the velocity structure is expected to be of second order importance and the rupture kinematics will control the nature of the ground motions. Therefore we feel that the parameters we have used are sufficient for characterizing fault-parallel (FP) and fault-normal (FN) ground motions time histories for the engineering application. Something to consider however is the fact that the simulations are based on linear-elastic theory and with very large near-fault ground motions some non-linear behavior may develop affecting actual ground motions.

The bridges that are studied have a natural frequency of 0.5 to 1 Hz, and important higher modes may be as high as 5 Hz. We use a grid discretization of 20m and based on the seismic velocities and 10 grid points per minimum wavelength the maximum frequency in the simulated ground motions, avoiding grid dispersion effects, is 17.5 Hz. This is well beyond the targeted spectral range of the modeled bridge. Since the simulated records are broadband from dc to the maximum frequency they are suitable for the engineering application. If we assume a more typical 5 grid points per minimum wavelength the maximum frequency is twice, however if lower seismic velocities are considered it will be reduced. The parameters we have used were chosen to allow for future higher resolution simulations incorporating lower seismic velocity if it is deemed necessary.

From the magnitude the fault length and width were determined to be 28.8 km, and 9.3 km respectively, based on Wells and Coppersmith (1994).

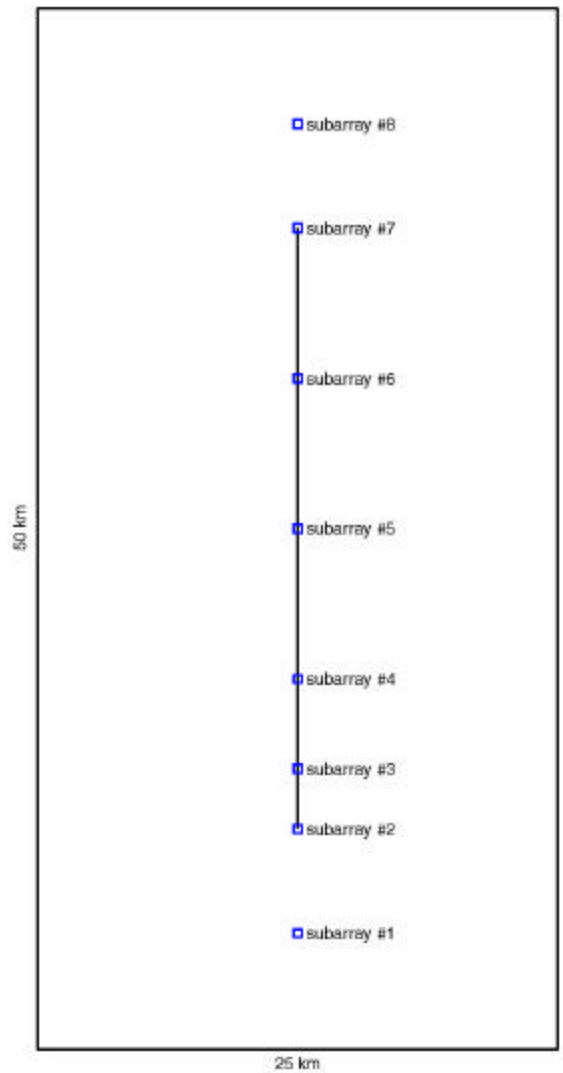

Figure 1. Map showing overall finite-difference model dimensions, and the location of the fault with subarrays of stations located along it. The hypocenter of the rupture model is located beneath subarray 3. Each subarray has several stations with the closest station 15m from the fault.

With this fault area and the scalar seismic moment obtained from the moment magnitude relationship the average slip on the fault is 0.71m.

0.71m is a large amount of differential offset for a bridge to accommodate. In our fault model if the fault does not reach the surface the differential offset across the surface projection of the fault would decrease. If the slip is not uniform, as is the case in real earthquakes there will be areas on the fault with greater or less slip than the average 0.71m (see the non-uniform slip modeling section for an example). Of course larger earthquakes have greater average and peak slip. It is important to keep these considerations in mind when examining the simulated time histories and the structural response of the bridge.

The finite difference model space is 50x25x15 km^3 and as Figure 1 shows the fault is centered in the model. The model dimensions are large to ensure that grid finiteness does not affect the simulation results by introducing reflection artifacts or errors in computing the static offset. The finite-difference grid has a spacing of 20m resulting in 2.3 billion grid points and a total required computer memory of 121.8 Gbytes. The simulations were run on a distributed memory super computer at the Lawrence Livermore National Laboratory.

Arrays of stations are located along the fault as shown in Figure 1. The subarrays each contain recording stations set at regular distance from the fault with the closest two stations each 15m from the fault. Subarrays 1 and 8 are off the ends of the fault, 2 and 7 are at the ends of the fault. The rest of the subarrays are located along the fault with the closest station only 15m from it. The hypocenter is located beneath subarray 3. Thus the rupture proceeds from south to north in Figure 1, from subarray 3 to 7.

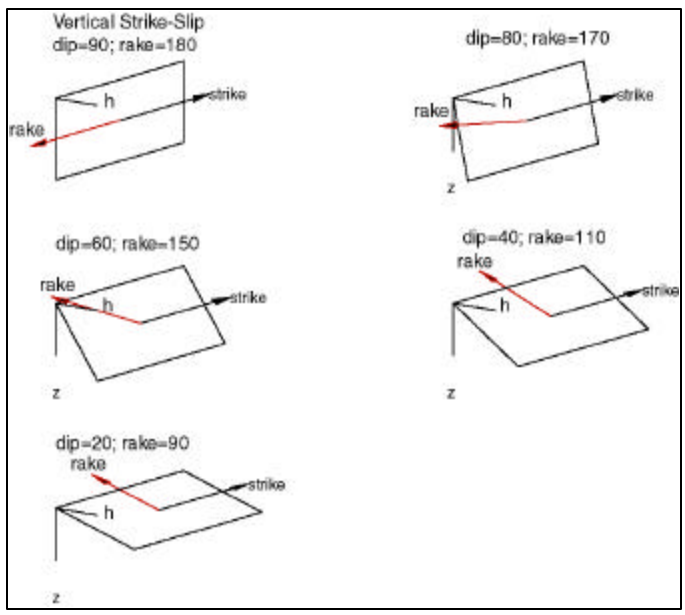

Figure 2. The five fault geometry models. “h” and “z” give the horizontal and vertical reference lines. In each case the dip and rake (slip direction in degrees) are listed. The strike and rake are shown as the black and red arrows, respectively.

We have performed five simulations systematically varying the dip and slip direction (rake) (Figure 2), while keeping the strike and all other model parameters (velocity model, rupture velocity, rise time) fixed. Because of space constraints we only present the vertical strike-slip results in this paper, which are shown in Figure 3.

Vertical Strike-Slip Results

The displacement seismograms at the closest station to the fault for each subarray are shown in Figure 3. Static offsets are observed on the FP component at sites adjacent to the fault. The static offsets are due to the sudden elastic rebound of the fault and are sometimes referred to as fling. The static offset on one side of the fault shows one-half of the total differential motion across the fault. The sign of the static offset is opposite at the stations on the other side of the fault. The FP component static offsets are reduced in amplitude at the two sites at the end of the fault (subarrays 2 and 7). This is due to the elastic response of the medium around the fault in which "push" and "pull" quadrants result in deformation that is not parallel to the fault strike. At these two sites, for the same reason, the FN component also shows a static offset. There are negligible static offsets at sites located off of the ends of the fault.

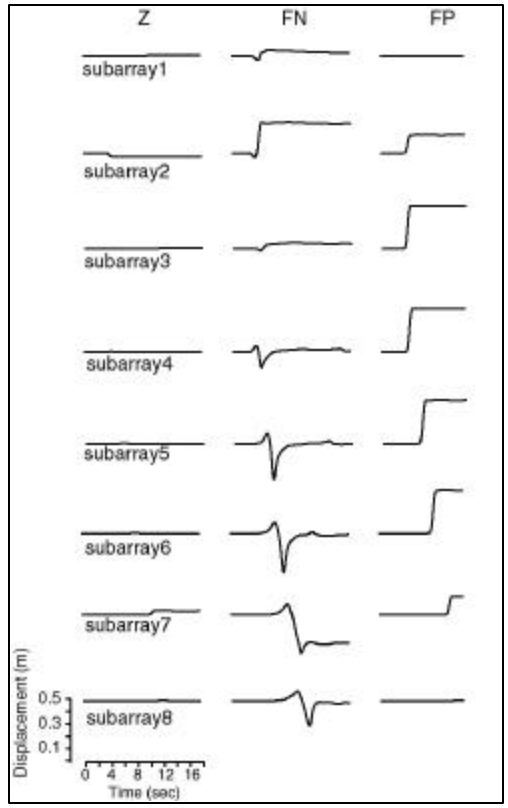

Figure 3. Comparison of three-component displacement records at subarrays 1-8 for the vertical strike-slip fault case. Rupture directivity is evident on the FN components. Constant amplitude static offsets are observed on the FP component for stations located along the fault.

The time from zero displacement to the final static value is controlled by the local slip rise time during rupture. In these simulations a constant average slip rise time from Somerville et al. (1999) was assumed. At such close distance to the fault the corresponding velocity pulses are representative of the local slip velocity during rupture.

The FN component on the other hand only has dynamic pulse-like motions with no static offset (except for the two fault end cases already discussed). The FN component has the same amplitude on each side of the fault like the FP component, but in contrast it also has the same sign. The pulse amplitude is seen to steadily grow from subarray 3 to 6 due to

directivity. At subarray 7 the FN amplitude is slightly reduced, and it remains large at subarray 8 off of the end of the fault.

Because the fault is vertically dipping and the slip direction is horizontal the vertical motions are very weak in comparison to the two horizontal components.

In Figure 4 the corresponding velocity records are compared. Large amplitude pulses are observed on each of the horizontal components. The FN velocity pulse is multi-lobed, while the FP velocity pulse is single-sided. The FN pulses show a strong directivity-controlled amplification, while the FP velocity pulses have constant amplitude along the length of the fault except at the two end points. This means that the proportion of FP to FN is variable along strike and therefore the total horizontal vector motion is also variable. In the case of dip-slip and oblique-slip cases the total vector motion along strike will also be variable because of the different behavior of fling- and directivity-controlled motions.

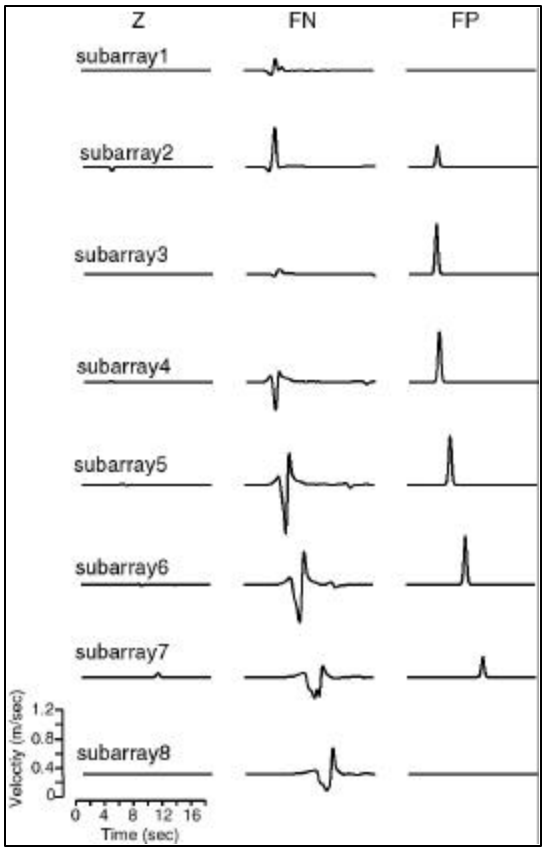

Figure 4. Comparison of three-component velocity records at subarrays 1-8 for the vertical strike-slip fault case. Rupture directivity is evident on the FN components. Constant amplitude velocity pulses are observed on the FP component for stations located along the fault.

The magnitude of the directivity effect depends on how co-linear the strike and slip directions are. In the case of a vertical strike-slip fault the strike and rake are co-linear producing a maximum directivity effect. In the case of a reverse fault the rake is perpendicular to the strike and this produces a minimum directivity effect (except in the updip direction). The simulations for the other fault orientations clearly illustrate this point. Figures 3 and 4 also show that the amount of directivity depends distance from the epicenter to the station.

In general the simulations show that both static offsets and dynamic directivity-controlled pulses need to be considered on any of the three components to account for possible faulting variability. In fact, as the faulting style trends to dip-slip cases there is increased vertical motions and a transition of fling-controlled motions (static offsets) to the FN component, and directivity-controlled motions to the FP component. In oblique

faulting cases it will be necessary to consider both dynamic pulses and static offsets in displacement on all three components.

There is also a pronounced hanging wall effect where motions at stations on the hanging wall are significantly larger as has been observed in the recent Chi Chi, Taiwan earthquake (Chi et al., 2001) and has been accounted for in regressions of strong ground motion observations (e.g. Abrahamson and Silva, 1997).

Non-Uniform Slip Simulations

A variable slip distribution will affect both the directivity component and also the static offsets, which will be proportional to the local fault slip and rise time. However, even in this case we expect the general shape of the near-fault time histories to remain pulse-like and quite similar to what is presented in this paper.

We are preparing for a final set of simulations in which the slip model and the rupture kinematics (rupture velocity and rise time) are variable over the fault surface. The first step is to obtain a suitable variable slip model for a Mw6.5 earthquake. To do this we used the method of Mai and Beroza (2002) to generate random spatial slip models. Figure 5 shows an example of a variable slip model appropriate for a Mw6.5 vertical strike-slip earthquake. The second step is to define the kinematic parameters namely, the rupture velocity and the slip velocity. Here we will assume a constant stress drop and slip velocity, and initially a constant rupture velocity. The assumption of constant slip velocity results in a model in which high slip regions take longer to achieve final offset compared to low slip regions. Thus in this model the rise time is variable. This is generally observed in studies inverting strong motion data for kinematic finite-source models.

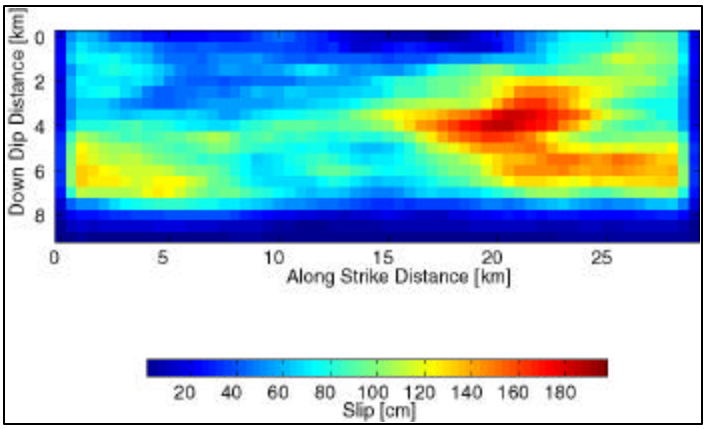

Figure 5. A random slip model for a Mw6.5 event based on Mai and Beroza (2002).

Summary and Conclusions

We have simulated near-fault time histories 15m from the fault for use in the analysis of fault-crossing bridges. These time histories are complete in terms of far- and near-field terms and therefore contain the effects of rupture directivity and fault fling. Rupture directivity produces strong displacement and velocity pulses that increase in amplitude in the direction of the rupture. The fling produces static offsets in displacement and single sided velocity pulses. At distances less than 100m both effects can be very strong.

In this study we have simulated motions for a range of fault types from vertical strike-slip to a 20-degree dipping thrust fault. The results of these uniform slip simulations show that the directivity and fling controlled waveforms occur on different components for each fault type. For a vertical strike-slip fault pronounced directivity is observed on the FN component, while nearly constant amplitude static offset in displacement and single-sided velocity pulses are observed on the FP component. In contrast, thrust type events show the static offset on the FN component with a weak directivity on the FP component, and also significant amplitude motions on the vertical component. Generally the results show that both static offsets and large amplitude velocity pulses need to be considered on all three components, and this is readily observed in the oblique rupture cases we considered.

For a vertical strike-slip fault the FN ground motions are the same on each side of the fault, whereas the FP component not surprisingly has equal amplitude but opposite static offset. This degree of symmetry disappears when the fault is dipping. Because a greater fraction of the fault surface is closer to the stations on the hanging block side of the fault (the side where the fault is dipping) the motions are larger. Both the dynamic and static motions are observed to be larger on the hanging block.

The amount of directivity depends on the length of the ruptured fault between the hypocenter and the recording station, the slip distribution along the rupture path, and the rupture velocity. The strong velocity pulses due to fault fling are to first order sensitive to the local slip and slip rise time on the fault.

Most of the simulations were for a rupture velocity 80% of the shear-wave velocity. Simulations were also performed for the vertical strike-slip case with rupture velocities equal to 70% and 140% of the shear-wave speed. In these simulations the FP, or fling-controlled motions were unchanged. There were significant differences to the FN, or directivity controlled motions.

Seismic velocity model complexity in the form of a velocity contrast across the fault, or a fault zone with a low velocity gouge are expected to be important in site-specific ground motions at sites located close to the fault or within the low velocity fault zone. Studies of fault zone guided waves have demonstrated a pronounced amplification of motions in the fault zone (e.g. Li et al., 1990; Benzion and Malin, 1991). These types of model complications are beyond the focus of the present study, but can be accounted for with our methodology.

The range of fault parameters that we have used to simulate near-fault ground motion time histories has revealed a rich behavior that is theoretically sound and consistent with the few existing near-fault records from real earthquakes indicating that the simulated time histories are suitable for use in the engineering analysis of fault-crossing bridges.

Acknowledgements

We wish to acknowledge Dr. Larsen (LLNL) for his help with the e3d elastic finite-difference code without which this study would not have been possible. The high-resolution simulations presented here were done on the MCR super computer at the Lawrence Livermore National Laboratory.

References

Abrahamson, N. A. and W. J. Silva (1997). Empirical response spectral attenuation relations for shallow crustal earthquakes, Seism. Res. Lett., 68, 1, 94-127.

Benzion, Y. and P. Malin (1991). San Andreas fault zone head waves near Parkfield, California, Science, 251, 1592-1594.

Chi, W.C., D. Dreger, and A. Kaverina (2001) Finite-source modeling of the 1999 Taiwan (Chi-Chi) earthquake derived from a dense strong-motion network, Dedicated issue on the Chi-Chi, Taiwan earthquake of 20 September 1999, Bull. Seism. Soc. Am., vol.91, no.5, pp.1144-1157.

Dolenc, D., D. Dreger and S. Larsen (2005). Basin Structure Influences on the Propagation of Teleseismic Waves in the Santa Clara Valley, California, Bull. Seism. Soc. Am., 95, 1120.

Dreger, D. S., L. Gee, P. Lombard, M. H. Murray, and B. Romanowicz (2005). Rapid Finite Source Analysis and Near-Fault Strong Ground Motions – Application to the 2003 Mw6.5 San Simeon and 2004 Mw6.0 Parkfield Earthquakes, *Seism. Res. Lett.* 76, 40-48.

Larsen, S. and C.A. Schultz (1995). ELAS3D: 2D/3D elastic finite-difference wave propagation code, Technical Report No. UCRL-MA-121792, 19 pp.

Li, Y. G., P. Leary, K. Aki, and P. Malin (1990). Seismic trapped models in the Oroville and San Andreas fault zones, Science, 249, 763-766

Mai, P. M. and G. C. Beroza (2002). A spatial random-field model to characterize complexity in earthquake slip, Journ. Geophys. Res., 107 (B11), 2308, doi:10.1029/2001JB000588.

Panning, M., D. Dreger and H. Tkalcic (2001). Near-source velocity structure and isotropic moment tensors: a case study of the Long Valley Caldera, *Geophys. Res. Lett*., 28, 1815-1818.

Somerville, P. G., K. Irikura, R. Graves, S. Sawada, D. Wald, N. Abrahamson, Y. Iwasaki, T. Kagawa, N. Smith, and A. Kowada (1999). Characterizing crustal earthquake slip models for the prediction of strong ground motion, Seism. Res. Lett., 70, 59-80.

Stidham, C., M. Antolik, D. Dreger, S. Larsen, and B. Romanowicz (1999). Three-dimensional structure influences on the strong-motion wavefield of the 1989 Loma Prieta earthquake, *Bull. Seism. Soc. Am.*, **89**, 1184-1202.

Wells, D. L., and K. J. Coppersmith (1994) New empirical relationships among magnitude, rupture length, rupture width, rupture area, and surface displacement, *Bull. Seism. Soc. Am.*, 84, 974-1002.